ACS APPLIED MATERIALS & INTERFACES

Research Article

www.acsami.org

Label-Free Water Sensors Using Hybrid Polymer–Dielectric Mid-Infrared Optical Waveguides

Pao Tai Lin,*[,†,§] James Giammarco,[‡] Nikolay Borodinov,[‡] Mykhailo Savchak,[‡] Vivek Singh,[†] Lionel C. Kimerling,[†] Dawn T. H. Tan,[§] Kathleen A. Richardson,[∥] Igor Luzinov,[‡] and Anu Agarwal[†]

[†]Materials Processing Center, Massachusetts Institute of Technology, Cambridge, Massachusetts 02139, United States

[‡]Department of Materials Science and Engineering, Clemson University, Clemson, South Carolina 29634, United States

[§]Photonics Devices and Systems Group, Singapore University of Technology and Design, Singapore 487372, Singapore

[∥]The College of Optics & Photonics (CREOL), University of Central Florida, Orlando, Florida 32816, United States

ABSTRACT: A chip-scale mid-IR water sensor was developed using silicon nitride (SiN) waveguides coated with poly(glycidyl methacrylate) (PGMA). The label-free detection was conducted at λ = 2.6–2.7 μm because this spectral region overlaps with the characteristic O–H stretch absorption while being transparent to PGMA and SiN. Through the design of a hybrid waveguide structure, we were able to tailor the mid-IR evanescent wave into the PGMA layer and the surrounding water and, consequently, to enhance the light–analyte interaction. A 7.6 times enhancement of sensitivity is experimentally demonstrated and explained by material integration engineering as well as waveguide mode analysis. Our sensor platform made by polymer–dielectric hybrids can be applied to other regions of the mid-IR spectrum to probe other analytes and can ultimately achieve a multispectral sensor on-a-chip.

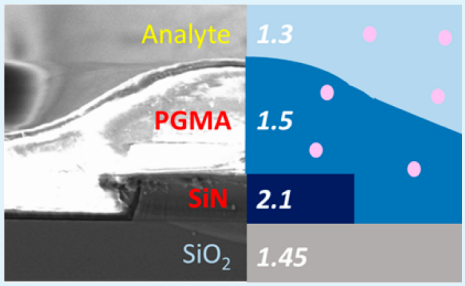

KEYWORDS: *mid-infrared absorption, label-free detection, hybrid polymer–dielectric waveguides, drop-cast coating, gradient refractive index, sensor on-a-chip*

INTRODUCTION

On-chip optical devices for chemical and biological sensing have attracted attention in recent years due to their small footprint, high-throughput detection, and capability to integrate with CMOS microelectronics.[1−4] Across a broad optical spectrum, the mid-infrared (mid-IR) regime between λ = 2.5 and 12 μm is of significant importance for optical sensing because characteristic absorptions of various chemical functional groups and molecular fingerprint signals reside here.[5−8] Thus, the concentrations and compositions of unknown chemicals can be identified by interpreting the spectral response from a mid-IR optical sensor. Among various mid-IR on-chip devices, waveguide-based sensors offer molecular fingerprinting for a large variety of chemical compounds via spectral measurements.[9,10] The output mode intensity from a low-loss waveguide attenuates according to the imaginary part of the refractive index (the absorption strength) of the surrounding analyte.[11,12] In other words, the spectral absorption information is encoded into the light transmitted through the waveguide. Unlike conventional sensors operating in the near-infrared region that can only inform us regarding concentration change without chemical identification, a mid-IR sensor offers unique advantages that can achieve analyses of both composition and concentration.[13,14]

Though chemical detection via mid-IR waveguide sensors have recently been demonstrated, there is an emerging need to improve their sensitivity to trace compounds that are highly toxic even in low concentrations.[15,16] Devices like waveguides with microring resonators and slot waveguides have been previously examined. However, a resonator, in comparison, can only be

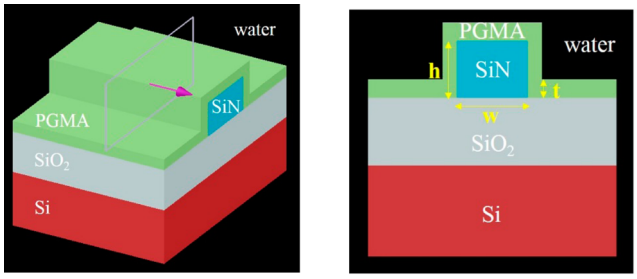

Figure 1. (a) The structure of the mid-IR hybrid waveguide that consists of dielectric SiN ridge with n = 2.1 and a layer of PGMA top cladding with n = 1.5. Since the PGMA has an intermediate index n between that of water and of SiN, it can effectively tailor the waveguide's evanescent field so that most of the field resides in the PGMA layer and surrounding water. The purple arrow indicates the direction of light propagation. (b) The cross-sectional schematic of the mid-IR hybrid waveguide. Structure parameters including waveguide width (w), waveguide height (h), and PGMA thickness (t) are indicated by yellow bars.

Received: February 4, 2015
Accepted: April 30, 2015
Published: April 30, 2015

DOI: 10.1021/acsami.5b01013
ACS Appl. Mater. Interfaces 2015, 7, 11189–11194

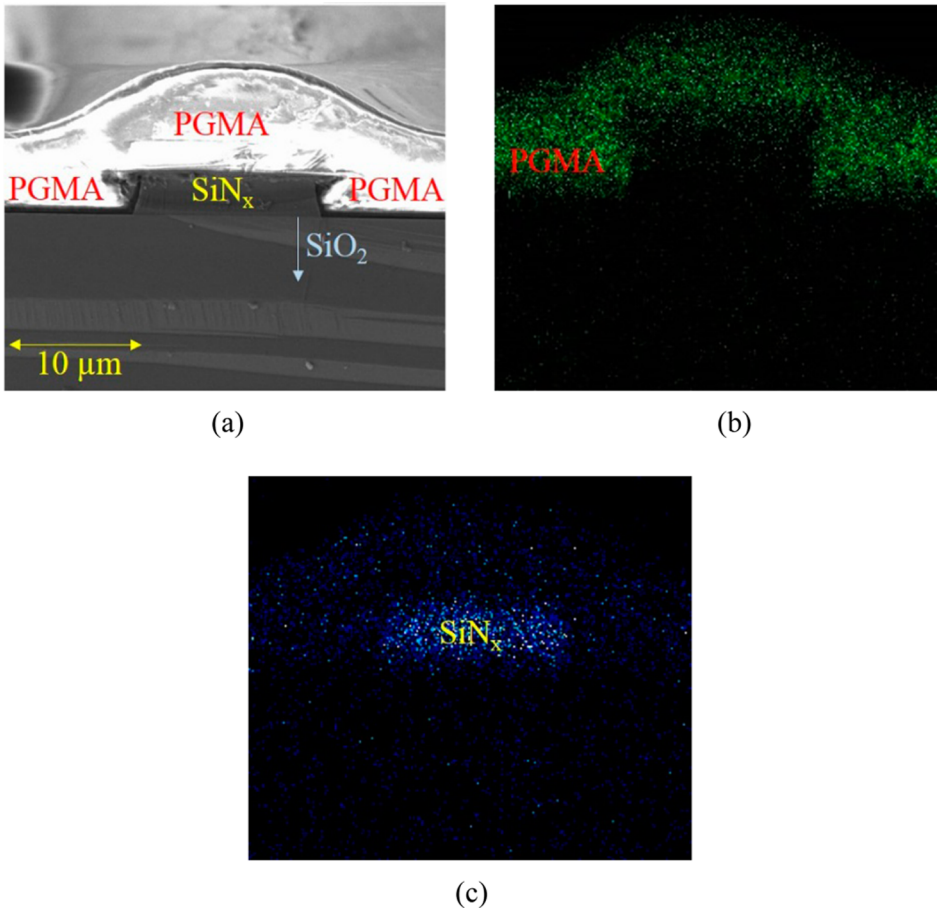

Figure 2. (a) The SEM image within the facet of a fabricated hybrid waveguide. The center is a SiN ridge covered by a layer of PGMA cladding. Underneath the hybrid waveguide is a SiO_2 buffer layer. Parts b and c are EDX images that indicate the amount and spatial location of carbon and nitrogen, respectively, corresponding to the PGMA layer and SiN ridge.

operated over a narrow and discontinuous spectrum due to strict resonance conditions and free spectral range. In addition, capturing changes at the output of a resonator requires a dedicated laser system with a tens of megahertz emission line width and sub-picometer step size.[17,18] Thus, utilizing microring resonators to perform broadband mid-IR scanning on a chip is impractical unless we also use an efficient tunable on-chip light source-cum-driver circuitry. Another technique utilizing slot waveguides that allows overlap of the mid-IR probe light with the analyte has been examined. Though enhancement of sensitivities has been observed, device preparation requires elaborate fabrication processes.

In this paper, we present a new mid-IR sensor platform that integrates dielectric and polymer media within an optical waveguide. The hybrid structure provides higher sensitivity because an enhanced interaction between the analyte and the probe light is achieved by altering the waveguide mode profile. The waveguide core is initially made from a high refractive index dielectric layer, so it can efficiently carry the mid-IR probe light. Later, the dielectric ridge is coated by a polymer that has a low refractive index because it is capable of reshaping the waveguide mode profile and expanding the evanescent wave into the polymer as well as the surrounding analyte. Due to the extended spatial overlap between the transmitted mid-IR light and the test analyte, the intensity modulation caused by analyte absorption is magnified and the sensitivity is improved accordingly.

EXPERIMENTAL METHODS AND DISCUSSION

Figure 1a illustrates the design of our polymer−dielectric hybrid waveguide, the water-sensing performance of which is tested at λ = 2.6−2.7 μm because water molecules have a strong O−H absorption at λ = 2.7−3.5 μm. The waveguide is composed of a dielectric silicon nitride ridge coated with a layer of poly(glycidyl methacrylate) (PGMA). SiN was chosen due to its broad mid-IR transparency up to λ = 8 μm, in addition to its low waveguiding loss. Meanwhile, the PGMA is the top waveguide cladding that improves water sensitivity through two means. First, PGMA has a refractive index (n) of 1.5, which is intermediate to those of water (n = 1.3) and SiN (n = 2.1 in our case). Due to PGMA's intermediate index, higher-order waveguide modes, wherein most of the optical field resides within the PGMA layer and the surrounding water, will be excited. Second, PGMA swells up to 1.2% as a result of exposure to water. This swelling introduces a spatial overlap between the mid-IR probe light and the absorbed water, enhancing light−matter interaction and thus strongly attenuating the transmitted mid-IR light. Between the SiN ridge waveguide and the Si wafer, there is an optical buffer layer of lower refractive index SiO_2 (n = 1.45) that prevents light leakage from the hybrid waveguide into the high refractive index Si substrate. Figure 1b presents a cross-sectional image where the structural parameters including waveguide width (w), waveguide height (h), and the PGMA thickness (t) are highlighted. The device geometry determines the sensor performance and

DOI: 10.1021/acsami.5b01013
ACS Appl. Mater. Interfaces 2015, 7, 11189−11194

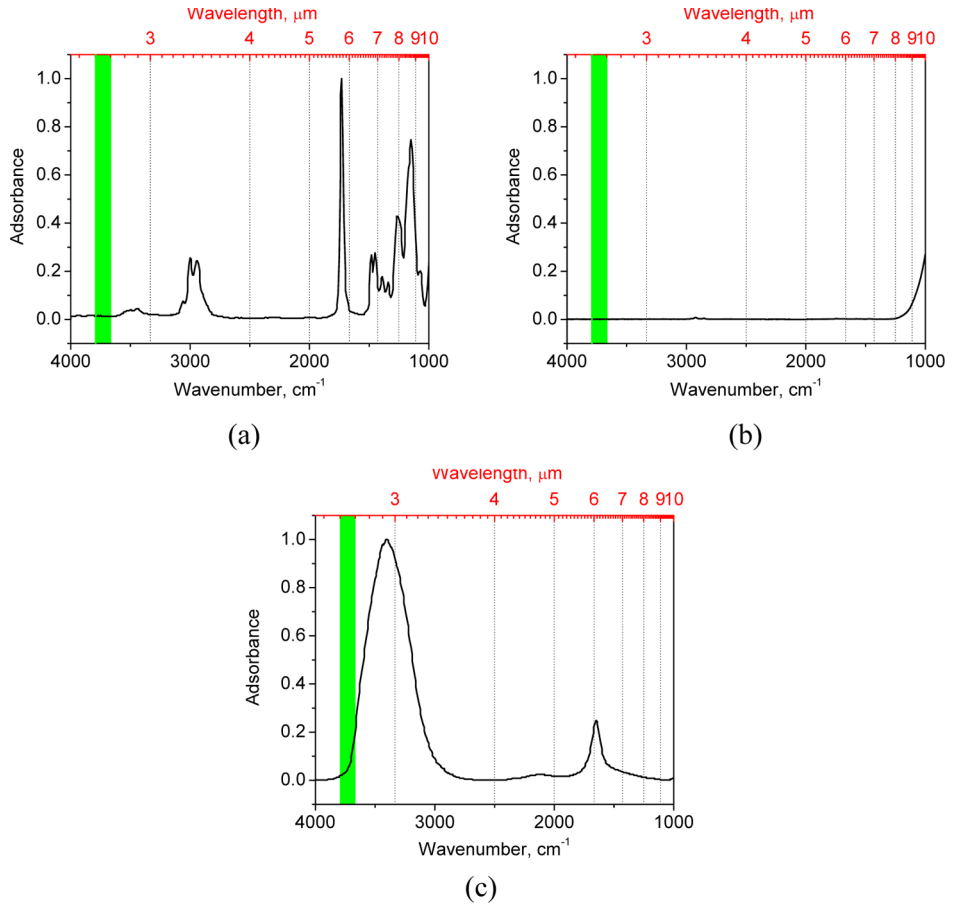

Figure 3. Infrared absorption spectra of (a) PGMA film, (b) SiN film, and (c) water analyte. Green bars highlight the spectral region (λ = 2.6–2.7 μm) transparent to our hybrid waveguide but overlap with the characteristic absorption of water molecules.

can be modified by pattern design, dielectric etching, and PGMA spin-coating methods.

The PGMA was synthesized through radical polymerization of glycidyl methacrylate (GMA), and it has a number-average molecular weight (M_n) of 352 000 g/mol.[19,20] SiN thin film was prepared via low-pressure chemical vapor deposition (LPCVD), and the ridge waveguide was fabricated using optical lithography and inductively coupled plasma-reactive ion etching (ICP-RIE). A 2% w/v PGMA in chloroform solution was drop-cast on the SiN waveguide, followed by solvent evaporation, with additional drying carried out using a nitrogen stream. The drop-casting procedure was repeated three times before annealing in a 120 °C vacuum oven for 12 h. Later, the sample was rinsed with chloroform three times to remove any unattached PGMA material. To characterize the water permeability into a PGMA polymer, swelling of PGMA layers upon adding water was conducted along with in situ ellipsometry; a 1.2% swelling expansion of PGMA was observed. The PGMA layer was fabricated as a thin, internally cross-linked film and covalently bound to the surface using its epoxy group functionalities.[21,22]

To characterize the morphology of the fabricated hybrid waveguide, SEM and energy-dispersive X-ray spectroscopy (EDX) images were captured at the waveguide facet. From the SEM image shown in Figure 2a, the SiN ridge waveguide is 2.5 μm tall and 12 μm wide; the waveguide width gradually shrinks into w = 4 μm toward the chip center. The taper structure is to improve the light-coupling efficiency between the waveguide and the external light source, and the taper is 500 μm long. The surface of SiN waveguide edges is found to be smooth, and that is critical in making a uniform polymer coating. A microns-thick PGMA layer is evenly in contact with the SiN ridge waveguide, while underneath the hybrid waveguide is the SiO_2 buffer layer. To better visualize the structure of the PGMA layer and the SiN ridge, EDX analyses, which maps the carbon from PGMA and the nitrogen from SiN, are utilized, and the resulting images are shown in Figure 2b,c. A well-defined PGMA cladding with a concave shape is observed, which indicates it conformally surrounds the SiN ridge placed in the center of the hybrid waveguide.

Mid-IR transparency of the synthesized PGMA polymer, SiN thin film, and analyte (water) is characterized by Fourier transform infrared spectroscopy with 64 scans, and their absorption spectra are shown in Figure 3a–c. For PGMA, a broad peak with low absorbance at 2.941 μm (3400 cm^{-1}) corresponds to the stretching of OH-groups that form during the PGMA annealing process; multiple peaks around 3.448 μm (2900 cm^{-1}) correspond to C–H stretching. A prominent peak at 5.780 μm (1730 cm^{-1}) is related to the vibrations of the carbonyl group. The SiN film is transparent from λ = 2.5 up to 8 μm, where the absorption after λ = 8.5 μm is due to Si–N stretching. Hence, our hybrid waveguide, consisting of both PGMA and SiN, is transparent between λ = 2.5 and 2.7 μm. On the other hand, the tested analyte (water) shows a broad and strong absorption at λ = 2.5–3.6 μm due to O–H stretches. From these absorption spectra, our PGMA–SiN hybrid waveguide is a suitable sensor platform for water detection, because the probe light at λ = 2.6–2.7 μm fits within the transparency window of the sensor and also matches the characteristic water absorption.

DOI: 10.1021/acsami.5b01013
ACS Appl. Mater. Interfaces 2015, 7, 11189–11194

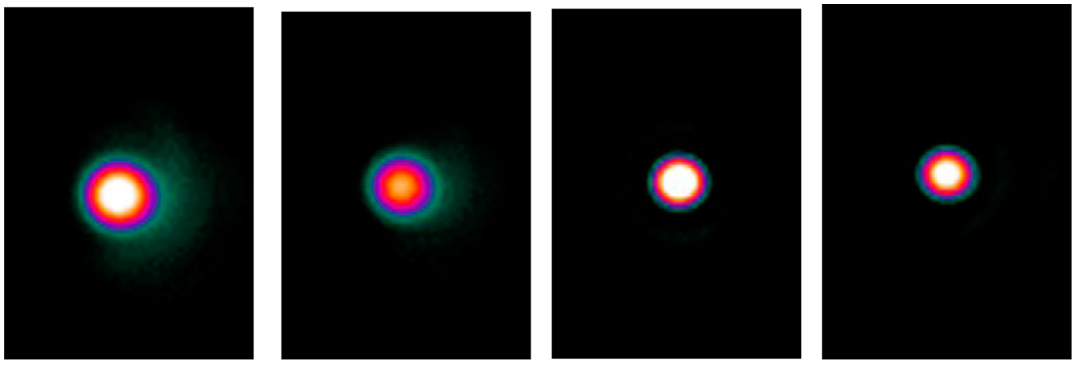

Figure 4. Mode images of PGMA−SiN hybrid waveguide (a) before and (b) after water exposure. Parts c and d are mode images from the SiN waveguide before and after water exposure, respectively. Large intensity attenuation is observed between parts a and b, whereas a trivial change is measured between parts c and d.

To evaluate the water-sensing performance, light intensity and mode profiles of mid-IR light passing through the mid-IR waveguides were characterized by a mid-IR indium antimonide (InSb) camera before and after dropping water onto the waveguide surfaces. The light source is a tunable mid-IR laser with a 10 ns pulse duration and 150 kHz repetition rate. The probe mid-IR light is coupled into the waveguide through a fluoride fiber with 9 μm core diameter. Since the fiber is wider than a single mode waveguide, it can efficiently generate a higher-order mode without the critical excitation condition. The wavelength of the probe light is selected at λ = 2.6−2.7 μm because PGMA and SiN are transparent in this regime, whereas water has a characteristic O−H absorption. Figure 4a,b is the measured mode images of the PGMA−SiN hybrid waveguide before and after water exposure, showing a clear intensity change that indicates that our hybrid waveguide has an agile response to water molecules. In contrast, a SiN waveguide without a PGMA coating is also evaluated via the same test process, and its mode profiles before and after adding water are shown in parts c and d of Figure 4, respectively. Unlike the hybrid waveguide, only a negligible difference is found between these two transmitted profiles, indicating that the SiN waveguide alone is unable to qualitatively detect the presence of water molecules with a high sensitivity. Thus, we demonstrate that by coating a SiN ridge waveguide with a PGMA layer, the performance of water detection can be significantly improved.

To better quantify the sensitivity improvement via PGMA coating, we measure the intensity profiles of light transmitted through the waveguide. Figure 5a shows the profiles from a PGMA−SiN hybrid waveguide before and after water exposure. Though the intensity distribution retains a Gaussian shape, a sharp drop of 38% was found in the intensity peak upon adding the water analyte. On the other hand, Figure 5b shows that the transmitted intensity from a SiN dielectric waveguide decreases by a mere 5% after water exposure. Thus, we demonstrate that the hybrid waveguide with a coated PGMA layer has an improved water sensitivity (by a factor of 7.6).

The improvement of water sensitivity can be explained by the optical waveguide modes associated with different structures. Figure 6 illustrates the electric fields calculated with the two-dimensional finite difference method (FDM). Figure 6a is the profile of a SiN ridge waveguide without a PGMA top cladding, whereas Figure 6b−d exhibits the profiles belonging to the fundamental mode and two higher-order modes of a PGMA−SiN

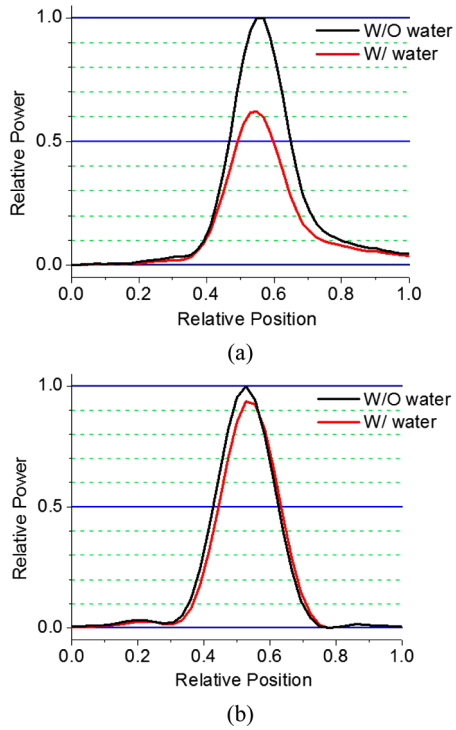

Figure 5. Intensity profiles of transmitted mid-IR light through different waveguides. (a) Profiles from PGMA−SiN hybrid waveguide before and after water exposure. A 38% attenuation is seen in the intensity peak. (b) Profiles measured from SiN dielectric waveguide before and after water exposure. Here, only 5% intensity change is observed.

hybrid waveguide. The 1.2% swelling of PGMA was taken into account in the simulation. For the fundamental mode (Figure 6a), the mid-IR light is well-confined within the SiN ridge, so only a weak evanescent field can actually interact with surrounding water analyte molecules. In contrast, higher-order modes reveal strong fields in the PGMA layer as well as extended evanescent tails into the surrounding water. The observed spatial overlap between the probe mid-IR light and the water molecules existing in PMMA layer and its surroundings introduces a strong light attenuation caused by water absorption. In addition, the gradient index profile can improve the excitation efficiency of the higher-order mode shown in Figure 6c,d. From our calculations, the relative absorption strengths of these four modes are

DOI: 10.1021/acsami.5b01013
ACS Appl. Mater. Interfaces 2015, 7, 11189−11194

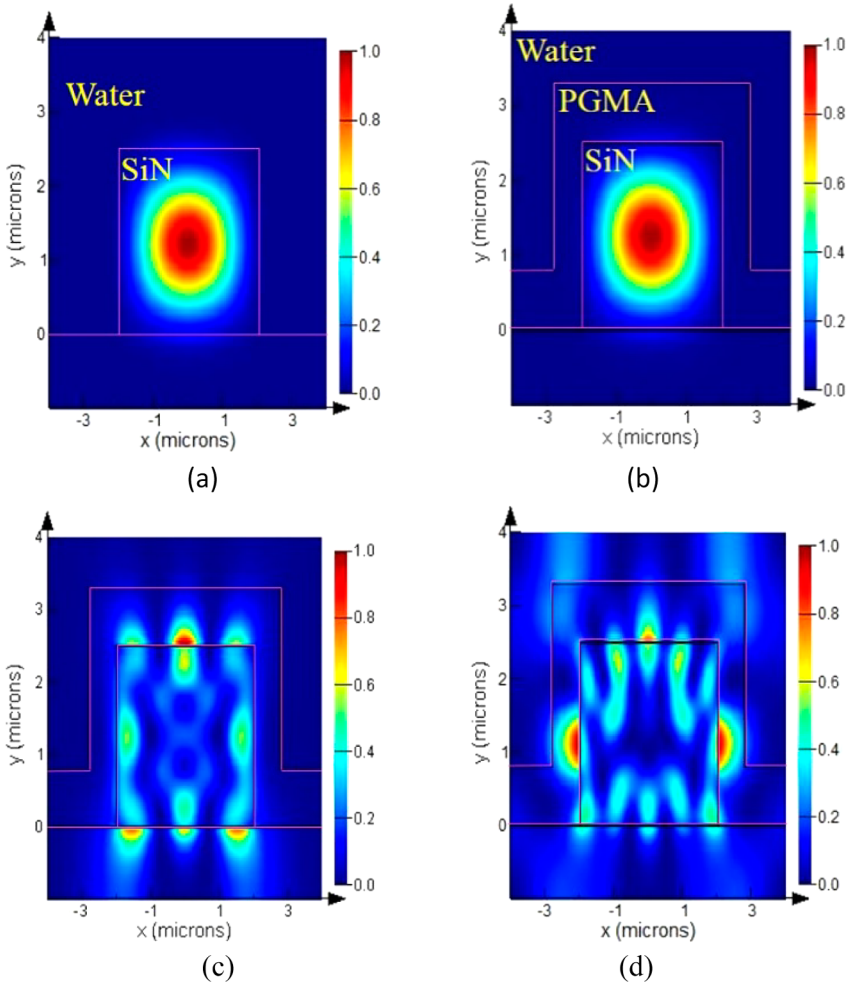

Figure 6. FDM-calculated electric field profiles for (a) a SiN ridge waveguide. A fundamental mode and two higher-order modes from a PGMA−SiN hybrid waveguide are shown in parts b and c, d, respectively. A strong field in PGMA and evanescent tails into the surrounding water are found in the higher modes.

0.051:0.001:0.112:0.673, which indicates that a higher-order mode will lead to larger intensity changes when water molecules surround the waveguide. The improvements of water sensitivity remain the same for various water concentrations. In brief, the presence of the PGMA coating causes higher-order modes to be created that subsequently improve the water sensitivity of the mid-IR waveguide for water detection.

CONCLUSION

In summary, we present a hybrid polymer−dielectric waveguide that can guide mid-IR light at $\lambda = 2.6-2.7\ \mu$m for label-free water detection. The resulting hybrid waveguide exhibited sensitivity that is 7.6 times higher than that of a conventional dielectric waveguide. The improvement of sensitivity is attributed to extensive spatial overlap between the mid-IR waveguide mode and the analyte. By coating a layer of PGMA on the SiN ridge, we create higher-order waveguide modes that bring a strong mid-IR field within the water swelling PGMA layer and expand the evanescent tails into the surrounding water. Our method of adopting material integration and waveguide mode engineering can accelerate the development of a mid-IR-based multispectral sensor-on-a-chip.

AUTHOR INFORMATION

Corresponding Author

*E-mail: paolin@mit.edu.

Notes

The authors declare no competing financial interest.

ACKNOWLEDGMENTS

Device fabrication was performed at Microsystems Technology Laboratories (MTL) at MIT, Center for Materials Science and Engineering (CMSE) at MIT, and Center for Nanoscale Systems at Harvard University. The authors acknowledge funding support from the Defense Threat Reduction Agency under award numbers HDTRA1-10-1-0101 and HDTRA1-13-1-0001. Funding for this work has been provided in part by the US Department of Energy (Contract # DE-NA000421).

REFERENCES

(1) Whitesides, G. M. The Origins and the Future of Microfluidics. *Nature* **2006**, *442*, 368−373.

(2) Gervais, L.; Rooij, N. d.; Delamarche, E. Microfluidic Chips for Point-of-Care Immunodiagnostics. *Adv. Mater.* **2011**, *23*, H151−H176.

(3) Chen, Y.-F.; Jiang, L.; Mancuso, M.; Jain, A.; Oncescuc, V.; Erickson, D. Optofluidic Opportunities in Global Health, Food, Water and Energy. *Nanoscale* **2012**, *4*, 4839−4857.

(4) Sloan, C. D. K.; Marty, M. T.; Sligar, S. G.; Bailey, R. C. Interfacing Lipid Bilayer Nanodiscs and Silicon Photonic Sensor Arrays for Multiplexed Protein−Lipid and Protein−Membrane Protein Interaction Screening. *Anal. Chem.* **2013**, *85*, 2970−2976.

DOI: 10.1021/acsami.5b01013
ACS Appl. Mater. Interfaces 2015, 7, 11189−11194

(5) Naumann, D.; Helm, D.; Labischinski, H. Microbiological Characterizations by FT-IR Spectroscopy. *Nature* **1991**, *351*, 81−82.
(6) Nasse, M. J.; Walsh, M. J.; Mattson, E. C.; Reininger, R.; Kajdacsy-Balla, A.; Macias, V.; Bhargava, R.; Hirschmugl, C. J. High-Resolution Fourier-Transform Infrared Chemical Imaging with Multiple Synchrotron Beams. *Nat. Methods* **2011**, *8*, 413−416.
(7) Chalmers, J. M.; Griffiths, P. R. *Handbook of Vibrational Spectroscopy*; Wiley: New York, 2002.
(8) Dam, J. S.; Tidemand-Lichtenberg, P.; Pedersen, C. Room-Temperature Mid-Infrared Single-Photon Spectral Imaging. *Nat. Photonics* **2012**, *6*, 788−793.
(9) Mizaikoff, B. Waveguide-Enhanced Mid-Infrared Chem/Bio Sensors. *Chem. Soc. Rev.* **2013**, *42*, 8683−8699.
(10) Ma, P.; Choi, D.-Y.; Yu, Y.; Gai, X.; Yang, Z.; Debbarma, S.; Madden, S.; Luther-Davies, B. Low-Loss Chalcogenide Waveguides for Chemical Sensing in the Mid-Infrared. *Opt. Express* **2013**, *21*, 29927−29937.
(11) Lin, P. T.; Singh, V.; Hu, J.; Richardson, K.; Musgraves, J. D.; Luzinov, I.; Hensley, J.; Kimerling, L. C.; Agarwal, A. Chip-Scale Mid-Infrared Chemical Sensors Using Air-Clad Pedestal Silicon Waveguides. *Lab Chip* **2013**, *13*, 2161−2166.
(12) Ryckeboer, E.; Bockstaele, R.; Vanslembrouck, M.; Baets, R. Biomedical Glucose Sensing by Waveguide-Based Absorption Spectroscopy on a Silicon Chip. *Opt. Express* **2014**, *5*, 1636−1648.
(13) Luchansky, M. S.; Bailey, R. C. Rapid, Multiparameter Profiling of Cellular Secretion Using Silicon Photonic Microring Resonator Arrays. *J. Am. Chem. Soc.* **2011**, *133*, 20500−20506.
(14) Zuta, Y.; Goykhman, I.; Desiatov, B.; Levy, U. On-Chip Switching of a Silicon Nitride Micro-Ring Resonator Based on Digital Microfluidics Platform. *Opt. Express* **2010**, *18*, 24762−24769.
(15) Chen, Y.; Lin, H.; Hu, J.; Li, M. Heterogeneously Integrated Silicon Photonics for the Mid-Infrared and Spectroscopic Sensing. *ACS Nano* **2014**, *8*, 6955−6961.
(16) Lin, P. T.; Kwok, S. W.; Lin, H.-Y. G.; Singh, V.; Kimerling, L. C.; Whitesides, G. M.; Agarwal, A. Mid-Infrared Spectrometer Using Opto-Nanofluidic Slot-Waveguide for Label-Free On-Chip Chemical Sensing. *Nano Lett.* **2014**, *14*, 231−238.
(17) Xia, Y.; Qiu, C.; Zhang, X.; Gao, W.; Shu, J.; Xu, Q. Suspended Si Ring Resonator for Mid-IR Application. *Opt. Lett.* **2013**, *38*, 1122−1124.
(18) Shankar, R.; Bulu, I.; Lončar, M. Integrated High-Quality Factor Silicon-on-Sapphire Ring Resonators for the Mid-Infrared. *Appl. Phys. Lett.* **2013**, *102*, 051108.
(19) Tsyalkovsky, V.; Klep, V.; Ramaratnam, K.; Lupitskyy, R.; Minko, S.; Luzinov, I. Fluorescent Reactive Core−Shell Composite Nanoparticles with a High Surface Concentration of Epoxy Functionalities. *Chem. Mater.* **2008**, *20*, 317−325.
(20) Liu, Y.; Klep, V.; Zdyrko, B.; Luzinov, I. Synthesis of High-Density Grafted Polymer Layers with Thickness and Grafting Density Gradients. *Langmuir* **2005**, *21*, 11806−11813.
(21) Iyer, K. S.; Luzinov, I. Effect of Macromolecular Anchoring Layer Thickness and Molecular Weight on Polymer Grafting. *Macromolecules* **2004**, *37*, 9538−9545.
(22) Zdyrko, B.; Klep, V.; Luzinov, I. Synthesis and Surface Morphology of High-Density Poly(ethylene glycol) Grafted Layers. *Langmuir* **2003**, *19*, 10179−10187.

DOI: 10.1021/acsami.5b01013
ACS Appl. Mater. Interfaces 2015, 7, 11189−11194